Chapter 6: Brittle Failure

THE DISTINCTION of *brittle* and *ductile* structures is of fundamental importance in geology. This is because ductile deformation involves penetrative strain, rotation, and displacement. In contrast, brittle deformation is principally caused by both rotation and translation of internally rigid blocks relative to one another. The rheological behavior of rocks can be studied quantitatively on the basis of laboratory experiments. The experiments fall roughly into two categories: *cold* (brittle) and *hot* (ductile) loading. Brittle behavior is discussed in this chapter. Ductile flow of rock, creep mechanisms, viscosity, creep laws, and deformation maps are outlined in chapters seven and eight.

Contents: Section 6-1 introduces the concept of rock failure by crack propagation. Uniaxial and triaxial loading tests are discussed in sections 6-2 and 6-3. The implications for the orientation of failure planes and joints are outlined in sections 6-4 and 6-5. The yield criterion of Mohr-Coulomb and the related friction laws of Amonton and Byerlee are outlined in sections 6-6 and 6-7. Crustal strength criteria are summarized in sections 6-8 and 6-9.

Practical hint: **Brittle failure of rock can be systematically investigated in rock mechanics laboratories, using uniaxial or triaxial rigs in cold press experiments. Visit such a laboratory, and perform or monitor one or more experimental runs.**

6-1 Crack propagation

Most lithologies deforming at the Earth's surface, with the exception of ice and salt, *cannot* flow in a ductile fashion. Any permanent deformation, accommodated by the grains and aggregates of crystals, occurs by their sliding past each other, as they fracture. Figure 6-1a illustrates the *cataclastic* or fractured fabric along an experimental fault in a sandstone. In nature, the friction on the fault plane may occasionally lead to, if fault movement is sufficiently fast, melting of the

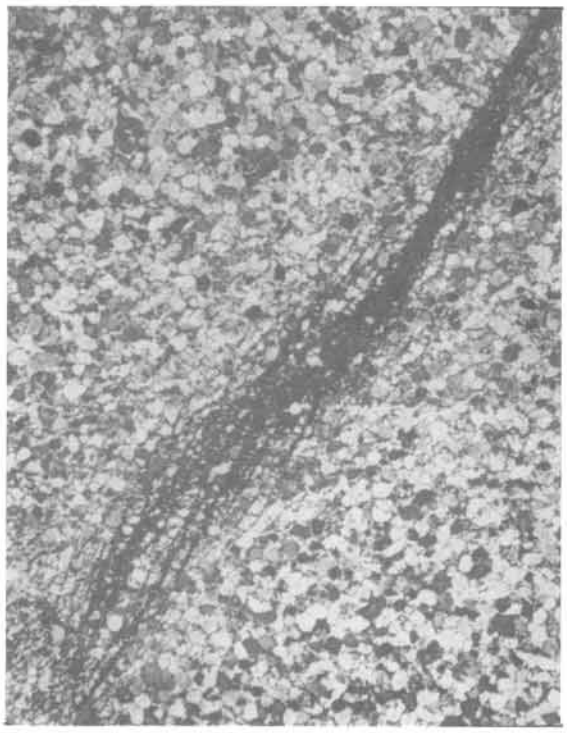

Figure 6-1a: *Reverse fault in St. Peter sand after 40% bulk shortening at 500 centigrade, 500 MPA confining pressure, and 100 MPa interstitial water pressure.*

wall rock. This is usually the case in rapid slip motions, associated with major earthquakes. The glass matrix remaining after rapid cooling of the melt as a thin film or vein on the fault plane, is termed a *pseudotachylite* (Fig. 6-1b). Pseudotachylites are usually not formed at the surface but at intermediate depths of about five to seven kilometers.

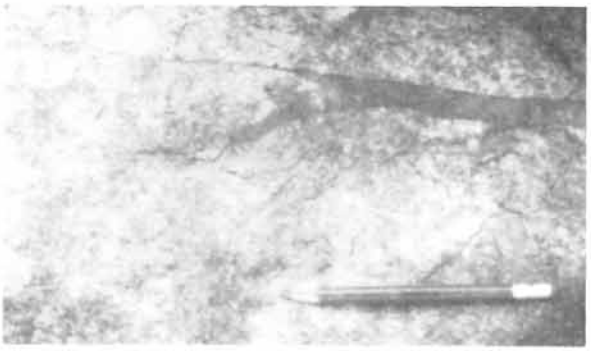

Figure 6-1b: *Pseudotachylite in Precambrian granite of the Arabian Shield, Khamis Mushayt, Saudi Arabia.*

Rock, an aggregate of mechanically bonded particles, contains numerous flaws, pore spaces, and microcracks. Microfracturing initiates at stress levels near the *peak strength*, *brittle strength*, or *yield strength* of a rock, marking the *elastic limit*. Evidence of fracture creation has been monitored from dilation and microseismicity in loaded samples. Once a minuscule fracture exists, stress concentrations at the crack tips (Fig. 6-2a & b) greatly facilitate propagation of the crack if properly oriented with respect to the directions of the principal stresses (Griffith's theory). Although crack propagation in laboratory experiments can occur at supersonic speeds, joint formation in nature is thought to occur by subcritical crack propagation. Joints propagate at subsonic rates, unless they are associated with either man-made instabilities or the rapid loading of an earthquake.

Although the cracks will initially be randomly oriented, according to *Griffith's theory*, the favorable direction of crack propagation will be normal to the direction of maximum tensile stress (Fig. 6-3a & b). Cracks perpendicular to the direction of maximum compression are likely to close and heal (in the absence of confining pressure). Experiments show that not all microcracks are present from the beginning of loading; some are formed during the loading itself. In multicomponent rocks, stress concentrations around grains of different elastic moduli may be responsible for forming microcracks. Planes of potential separation in rocks are created by the crack propagation, aided by the locations of pore spaces, noninterlocking grain boundaries, and intracrystalline weaknesses, such as kink-bands and glide lamellae. Porosity varies from 50 to 10% volumetric pore space in soils, sands, and limestones and from 20 to 5% in sandstones. It is less than 5% in shales and is commonly less than 1% in crystalline rocks with interlocking grain boundaries. Clearly, crystalline rocks have the largest possible yield strength and soils have a negligible yield strength.

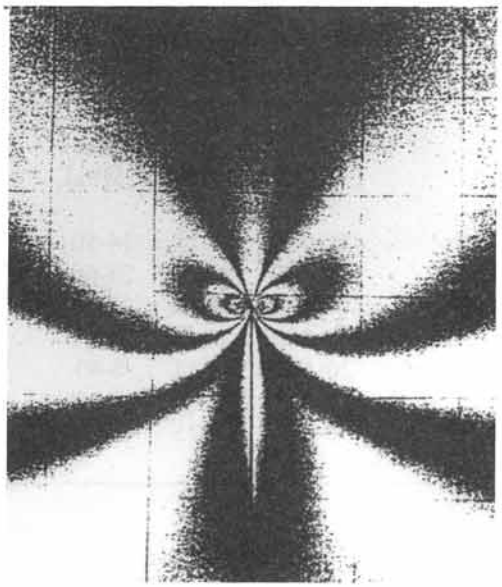

Figure 6-2a: *Isochromatic fringes in photoelastic plastic, subjected to vertical shortening. The crack propagates at 400 m s^{-1}. The grid spacing is 2.5 cm.*

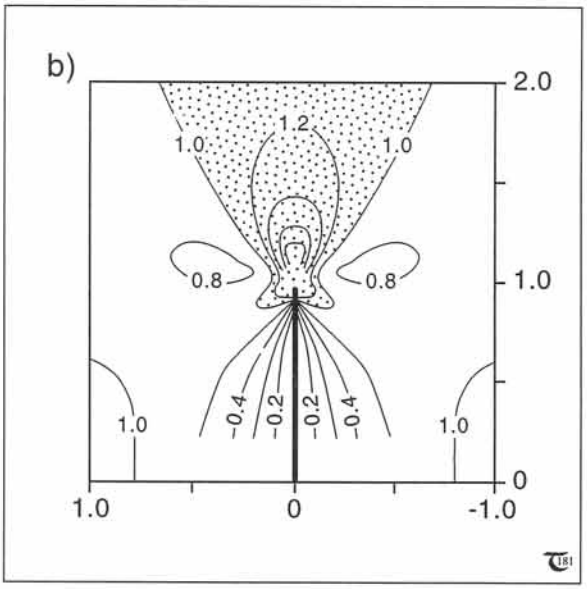

Figure 6-2b: *Contours of shear stress magnitude, similar to isochromatic fringes in photoelastic materials. The stress concentrations are largest near the tip of the propagating crack (shaded).*

□Exercise 6-1: Study carefully the stress distribution of Figure 6-2b, and determine the locations where the difference between the major and minor principal stresses must be maximum and minimum, respectively.

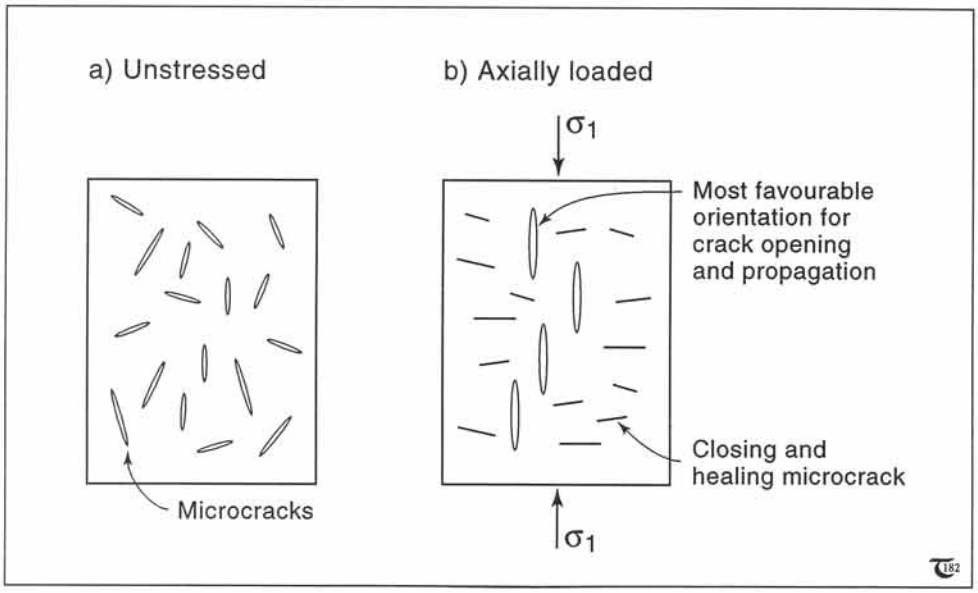

Figure 6-3: *a) & b) Griffith's crack propagation model. (a) Randomly oriented micro-cracks in the undeformed continuum. (b) Upon loading, only those micro-cracks, which are favorably oriented, may open and propagate.*

6-2 Uniaxial tests

Unconfined compressive rock strength is determined by *uniaxial shortening* of circular cylinders of length/diameter ratio 2 to 2.5 (Fig. 6-4), carefully prepared and step-loaded at a rate less than 0.7 MPa s^{-1} (see exercise 5-7). The unconfined strength for rocks varies between 10 MPa for weathered rocks to about 500 MPa for fine-grained crystalline rocks (Table 6-1). Contours of tensile deviatoric stress magnitude, normalized by the load stress, in a vertical plane through the axis of a uniaxially loaded sample, are shown in Figure 6-5.

Table 6-1: *Brittle failure strength for rocks stressed under atmospheric pressure.*

Rock	Compression (MPa)	Tension (MPa)	Shear (MPa)
Granite	100-250	7-25	14-50
Dolerite	100-350	15-35	25-60
Basalt	100-300	10-30	20-60
Quartzite	150-300	10-30	20-60
Sandstone	20-170	4-25	8-40
Shale	5-100	2-10	3-30
Limestone	30-250	5-25	10-50

The typical failure curve plots the stress versus the strain, in a so-called constant strain-rate test (Fig. 6-6). Five stages in the failure process can be distinguished: a) Microcracks and pore spaces, oriented at suitable angles with respect to the applied stress, will close at the onset of loading, causing an initial non-recoverable strain non-linearity in some rock samples. b) Sub-sequent elastic distortion in Poisson mode occurs with almost no microseismicity. c) & d) The first propagation of microcracks, formation of new microcracks, and associated *microseismicity*, and partially recoverable elastic volume *dilation* occur after stress levels reach about 50% of the peak strength, with a dramatic increase at 80% stress of the peak strength. e) The stress drops after the brittle strength has been reached, a process termed *strain softening*, which is due to coalescence and forking of microcracks into macroscopic fractures, but the rock remains intact. f) The stress reaches a plateau value characteristic for frictional plasticity, termed the *residual strength*, marking the complete separation of rock portions

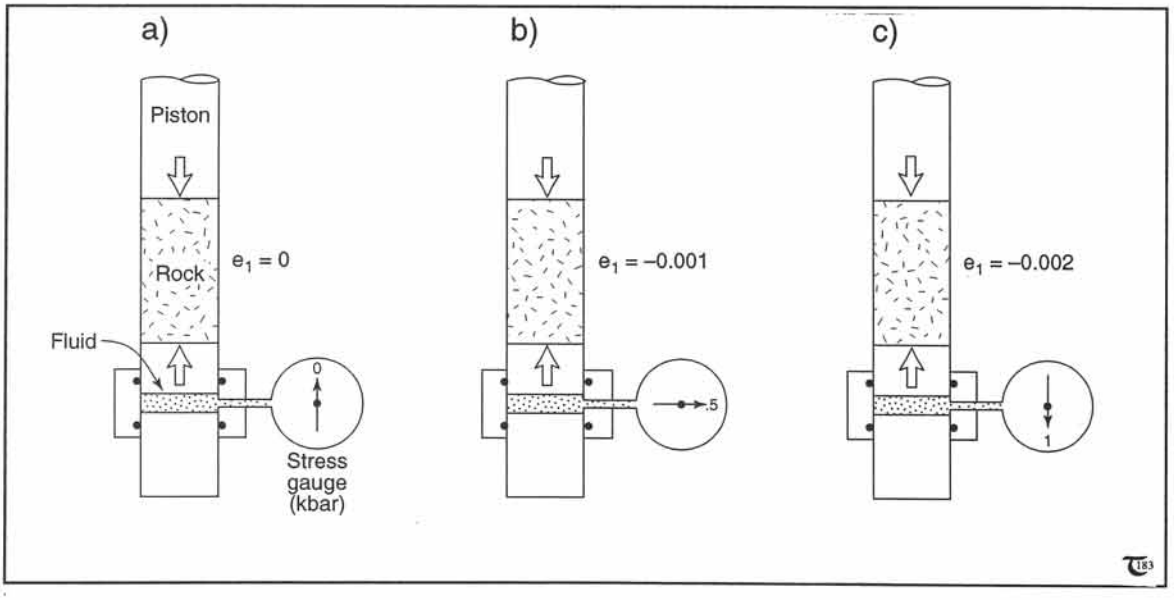

Figure 6-4: *a) to c) Sections through a uniaxial press. The confining pressure remains atmospheric, because the lateral sample movement is not constrained.*

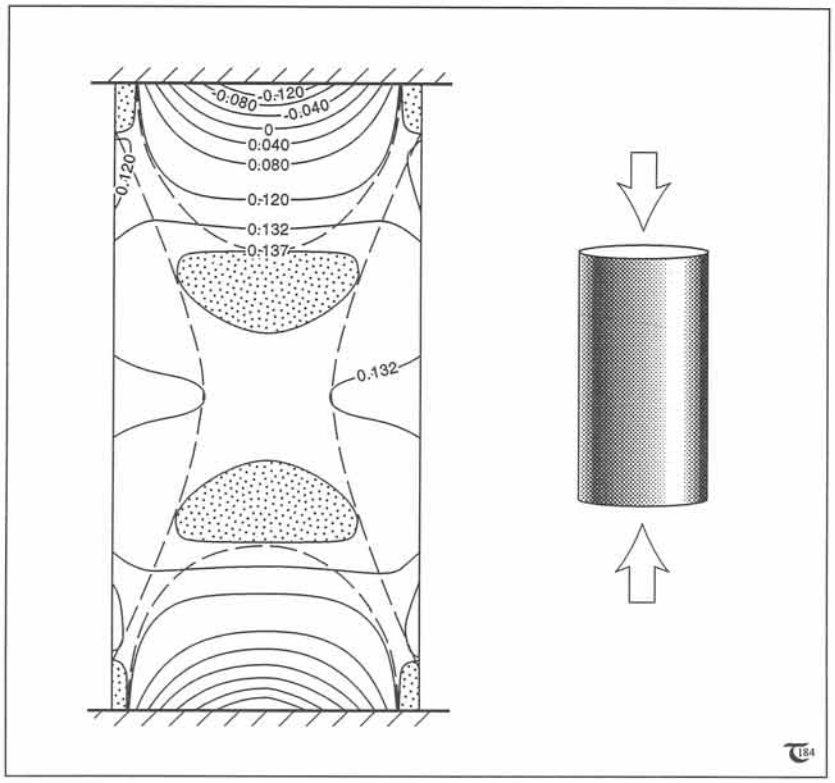

Figure 6-5: *Contours of normalized deviatoric stress magnitude in vertical plane along the axis of a uniaxially loaded sample. The section prone to shear failure is between the dashed lines.*

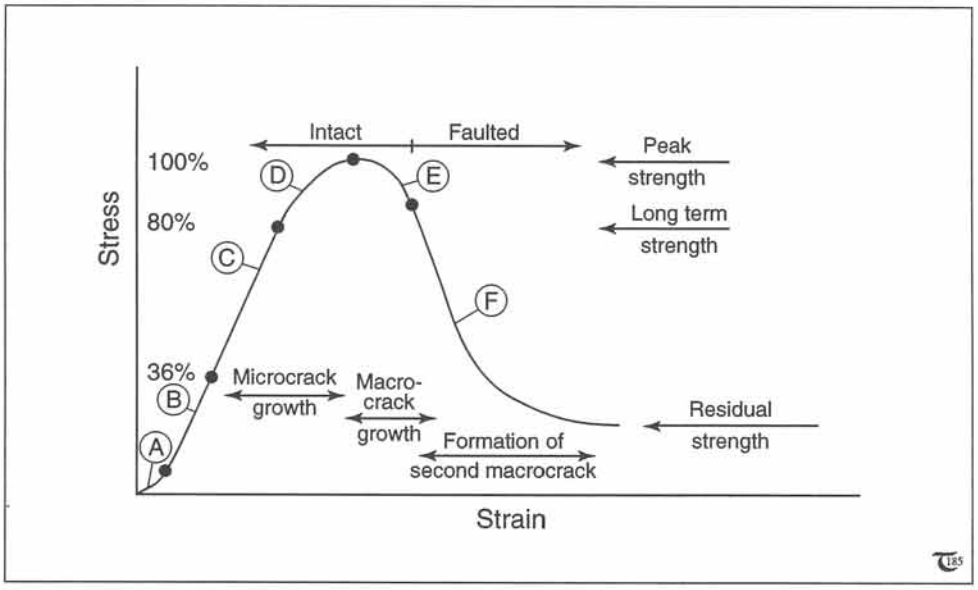

Figure 6-6: *Typical stress-strain diagram for cold press test on rock sample, initially deforming elastically, followed by structural failure and frictional slip. See text for discussion of stages a) to f).*

(Continued from p. 82) in the test sample. The rock is then said to contain discontinuity planes, fissures, ruptures, cracks, or fractures. Such cracks are termed faults only if slip movement has occurred on them.

☐Exercise 6-2: The process of rock failure, including anelasticity, can be approximated by combining the mechanical analogs of Figures 5-1d and 5-16b, as illustrated in Figure 6-7. Determine which of the individual components correspond to which stage in the failure process.

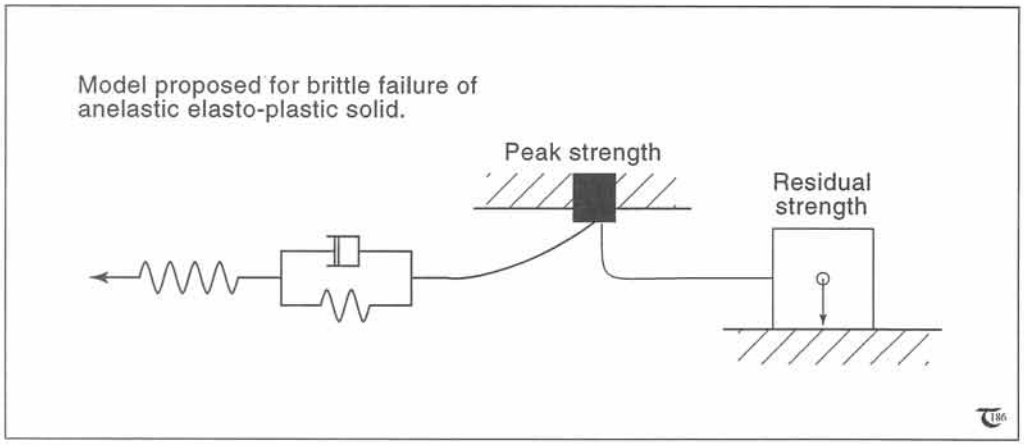

Figure 6-7: *Mechanical analog, made up of a standard linear solid, peak-strength plug and frictional-plastic unit. This analog model simulates the behavior seen in the stress-strain graph of Figure 6-6.*

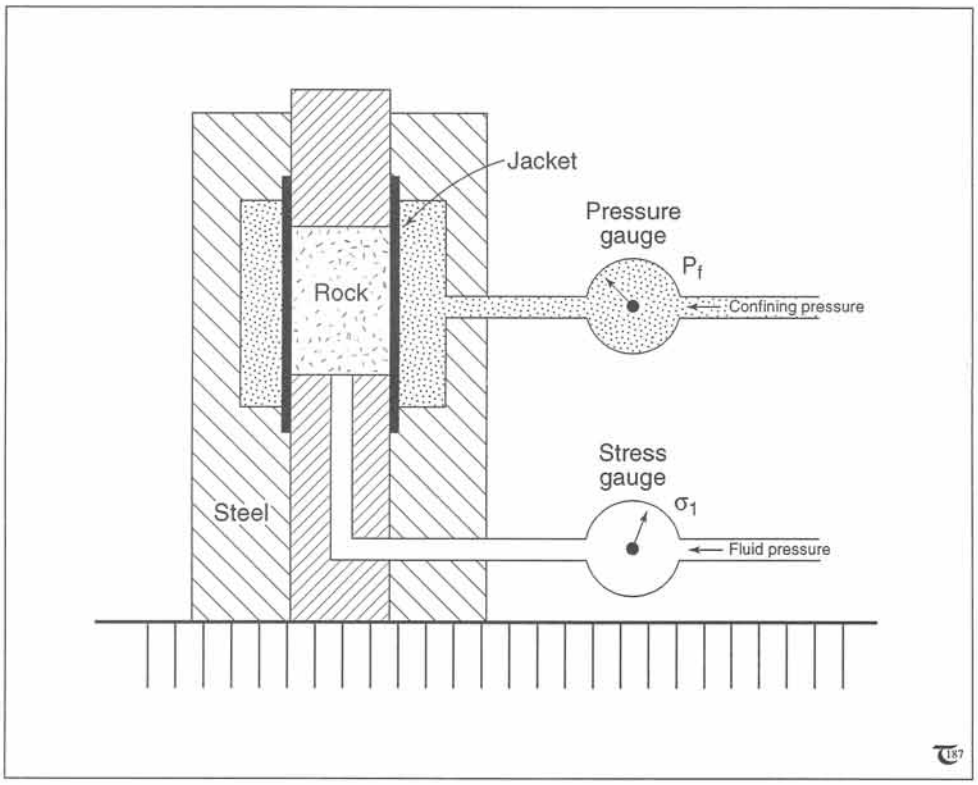

Figure 6-8: *Section through a triaxial deformation rig, also termed Griggs apparatus. Samples are sealed by a brass jacket and hydraulically pressurized from the sides while subjected to vertical loading.*

6-3 Triaxial tests

Triaxial testing is done very similarly to uniaxial testing, except that a confining pressure, P, can be imposed (Fig. 6-8), whereas P necessarily remained negligible in uniaxial tests because of the free lateral boundaries. If all three principal stresses applied are larger than zero, a confining pressure arises, equal to their arithmetic mean value. The results of triaxial stress tests are usually represented in graphs plotting percentage strain versus the *stress difference*, defined as $(\sigma_1-\sigma_3)$. The stress difference is, also, termed differential stress, but it is not differential in the mathematical sense. The stress values are usually selected such that $|\sigma_1| > |\sigma_2| = |\sigma_3|$, and P equals σ_2. The effect of increasing pressure is that the strain softening, typically monitored at low pressures, disappears, and frictional plasticity or cataclastic flow occurs immediately after the brittle strength has been reached (Fig. 6-9). Compare Figures 6-6 and 6-9, and notice that the strain-softening (or drop in stress) upon failure decreases when rocks are deformed under higher, confining pressures.

The brittle strength itself, naturally, also, increases at higher confining pressure, because it becomes more difficult for microcracks to open and propagate (Figs. 6-9 and 6-10). The residual strength or stress, required for frictional plasticity, simply is higher, because the confining pressure increases the normal stress perpendicular to any potential glide surface. It is important to realize that *crystalline or ductile creep is not observed in most rocks deformed at room temperatures*, unless the confining pressure is increased to extremely high values of over 1000 MPa. Those conditions are not likely to occur normally in crustal rocks, unless exposed to meteoritic impact or crypto-explosions. Exceptions are ice and rock salt, which display crystalline creep at much lower temperatures and pressures than other rocks.

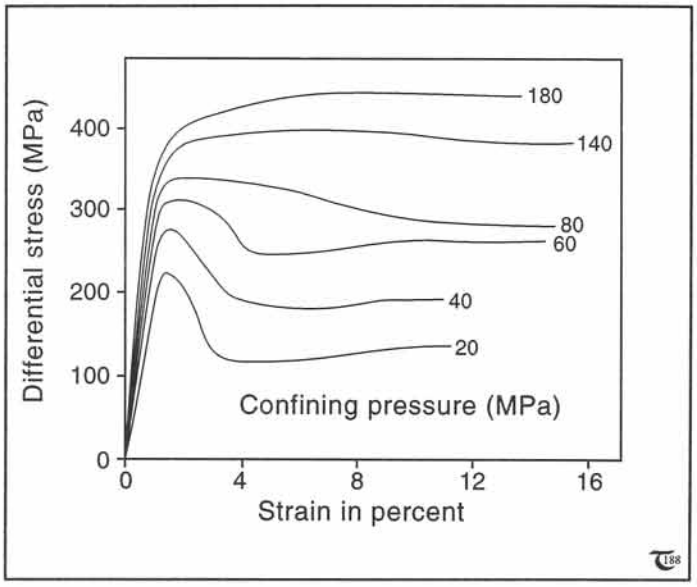

Figure 6-9: *Typical stress-strain diagram for cold press tests of pyroxenite samples at elevated, confining pressures.*

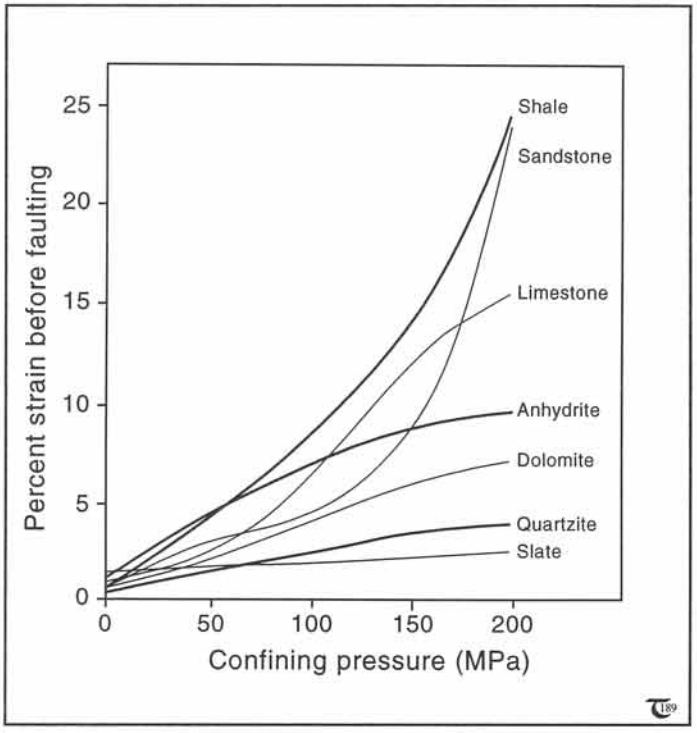

Figure 6-10: *Macroscopic, brittle failure occurs at larger critical strains if the confining pressure increases. This is because the opening of microcracks is inhibited at increased pressures.*

☐Exercise 6-3: Study the failure curve of Figure 6-6 recorded with the *uniaxial load apparatus* (Fig. 6-4), at atmospheric pressure. Compare this curve with the set of failure curves of Figure 6-9, recorded with a *triaxial deformation apparatus* (Fig. 6-8). Make sure you understand the mechanical model of Fig. 6-7, and explain which mechanical element can be removed from the model for failure curves at high confining pressure.

☐Exercise 6-4: Figure 6-10 shows the effect of increased confining pressure upon the amount of strain (and thus the peak stress) required before failure occurs in triaxial tests. a) Plot a depth scale on Figure 6-10, corresponding to the confining pressures indicated. b) At depths corresponding to 25 MPa, the amount of strain required to break or fail (the peak strength of) anhydrite is higher than that of sandstone. What is the triaxial relationship at 150 MPa? c) Discuss whether sandstone faults before or after limestone and at which depths.

6-4 Orientation of failure planes

Failed rock contains *discontinuity planes*, termed fissures, ruptures, cracks, or fractures, if no significant shear displacement has taken place along the separation plane. Regularly spaced and subparallel sets of fractures in nature are termed *joints*. Some joints display minor displacements and, therefore, are minor shear faults. It is important to infer the orientation of the principal stress axes with respect to the fracture planes from laboratory tests in rock mechanics. True fractures without fault displacement, or *tension joints*, are formed perpendicular to the

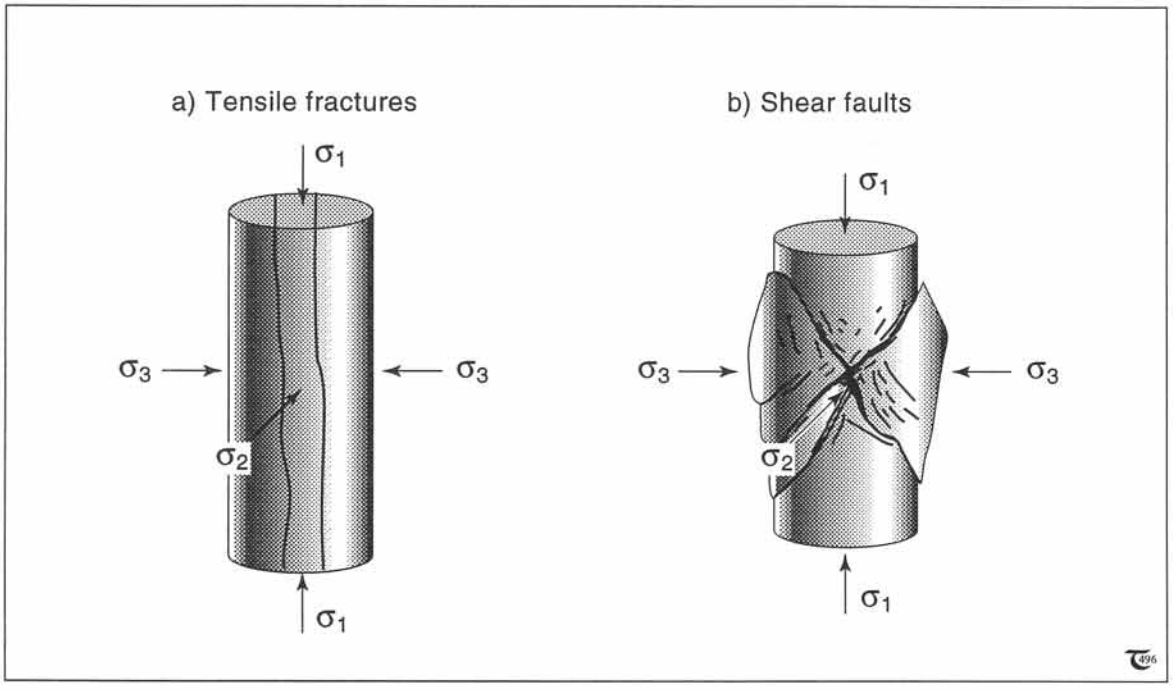

***Figure 6-11:** a) & b) The orientation of tension joints and shear faults with respect to the principal stresses. (a) Low or zero σ_3, (b) high σ_3 (see, also, Fig. 6-20).*

least principal stress axis, σ_3, and parallel to the σ_1-σ_2-plane (Fig. 6-11a). Movement over the fracture is impossible under the prevailing stress field responsible for its creation, because the critically resolved shear stress for this fracture orientation is zero (cf. equation 4-6b).

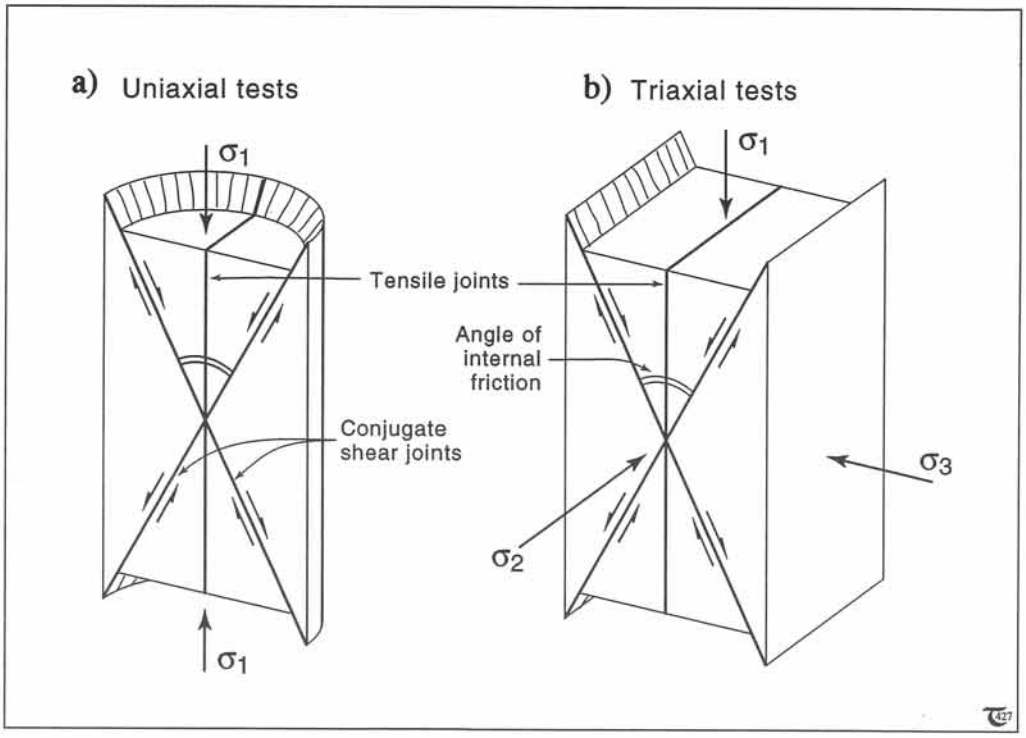

Figure 6-12: a) & b) Tension joints and shear joints in deformation tests.

In contrast, *shear joints* form close to the direction of maximum shear stress, which is in two conjugate planes at 45° to σ_1 and σ_3 (Fig. 6-11b). It has already been discussed in section 3-3 that the angle of internal friction of most rocks is closer to 30° to 40° rather than 45°. The Mohr-Coulomb criterion, introduced later, does not predict that the planes of shear failure follow the maximum shear stress planes; failure planes are predicted to follow planes at an acute angle to σ_1, as observed.

☐Exercise 6-5: In some rock failure tests, shear faults and tension joints may form simultaneously. Figures 6-12a & b idealize the failure surfaces. The shear failure sometimes may follow a conical surface, as outlined in Figure 6-12a, but the occurrence of two discrete, conjugate failure planes is more common (Fig. 6-12b). Explain why the conical shear failure occurs in some tests but not necessarily in all tests.

6-5 Joints

The rate of crack propagation in nature can occur at supersonic speeds, as is evident from the audible seismicity, accompanying rock failure incurred by explosive blasting in quarries and at roadcuts. Failure surfaces thus induced, as well as natural joint surfaces, inherit remarkable surface markings, including so-called *arrest lines*, which help to constrain the direction of fracture propagation (Fig. 6-13). Joints are commonly observed in the upper kilometer of granite plutons, sometimes subparallel to the outcrop surface, causing separation of large slabs, a process termed sheeting (for large-scale separation) or exfoliation (for small-scale separation) (Figs. 6-14a & b). Similarly, hexagonal columnar jointing with Y-intersections is typically observed in basaltic sills, dikes, and lavas, created by thermal stresses, associated with rapid cooling after their igneous emplacement (Figs. 6-15a & b). Cooling of the subparallel boundaries of basaltic sheets starts at the margins, where thermal contractional

stresses support volume changes. Shortening normal to the principal cooling surface can be accommodated uniformly by lowering of the top surface. However, lateral shrinkage can be achieved only by the growth of vertical cracks, thus explaining the formation of columnar joints.

Spectacular examples of regional jointing, confined to subhorizontal sandstones, occur in the Entrada Formation near Moab, Utah (Figs. 6-16a & b) and in the Cedar Mesa rocks of Canyonlands National Park, Utah (Fig. 6-16c). The two sets of joints seen in the Entrada Formation are separated by only 10°. It seems that E-W extension has occurred with a late clockwise shift of the paleostress axes, causing a new N-S joint set, overprinting and cross-cutting the other, older set at 10°. The apical angle between the two joint sets in the Cedar Mesa is about 70° and may well be a conjugate set of shear failure planes with little displacement, each set oriented at 35° with respect to the major principal stress axis. On the other hand, the up-down joint set abuts the upper right to lower left joint set a number of times. Some geoscientists would suggest that shear fractures do not abut in this manner, because they must all abut with no exceptions. Also, cross-joints commonly resemble shear fractures, but may be created by mechanisms other than conjugate shear fracturing, including the relaxation of thermal stresses.

☐Exercise 6-6: a) How much will a 100 meter stretch of a basalt flow shorten as it cools from 1000° C to the average ambient surface temperature of 25° C, given a thermal expansion coefficient of 2.5×10^{-6} $C^{\circ -1}$? b) Is the jointing due to surface or body forces?

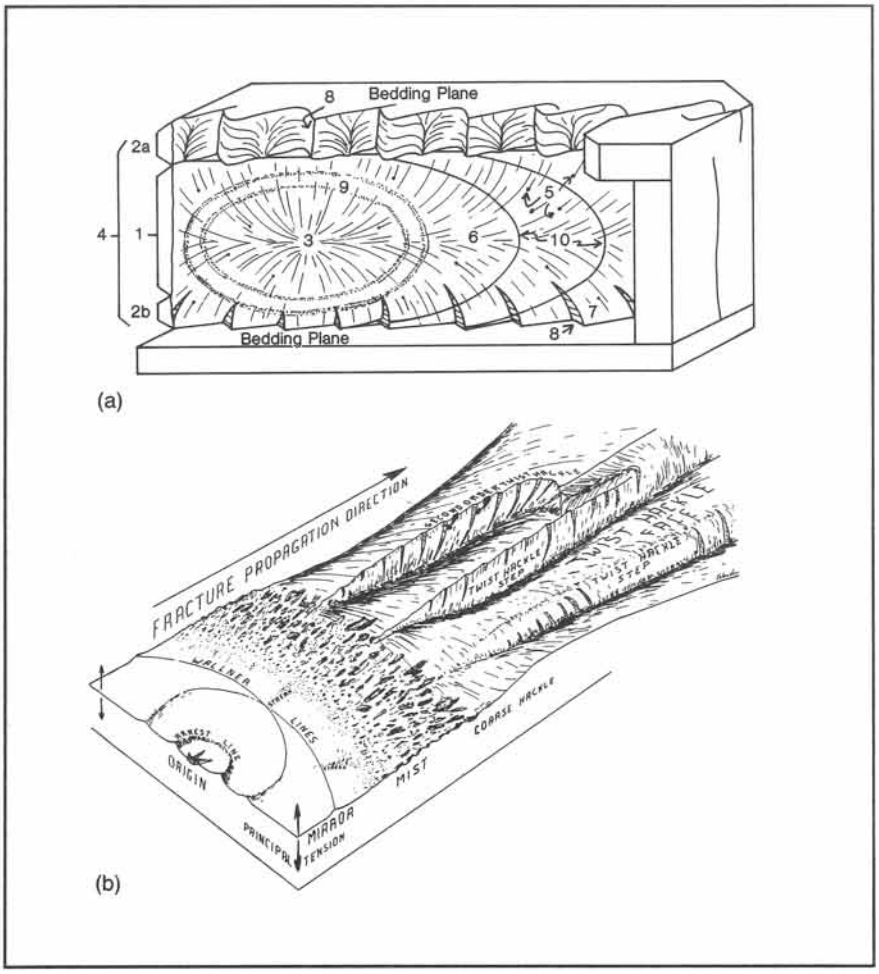

Figure 6-13:
a) Variety of markings seen on joint surfaces: (1) main joint face, (2) twist hackle fringe, (3) origin, (4) hackle plume, (5) inclusion hackle, (6) plume axis, (7) twist-hackle face, (8) twist-hackle step, (9) arrest lines, and (10) constructed fracture-front lines.
b) Additional terms and features of propagating joint surfaces.

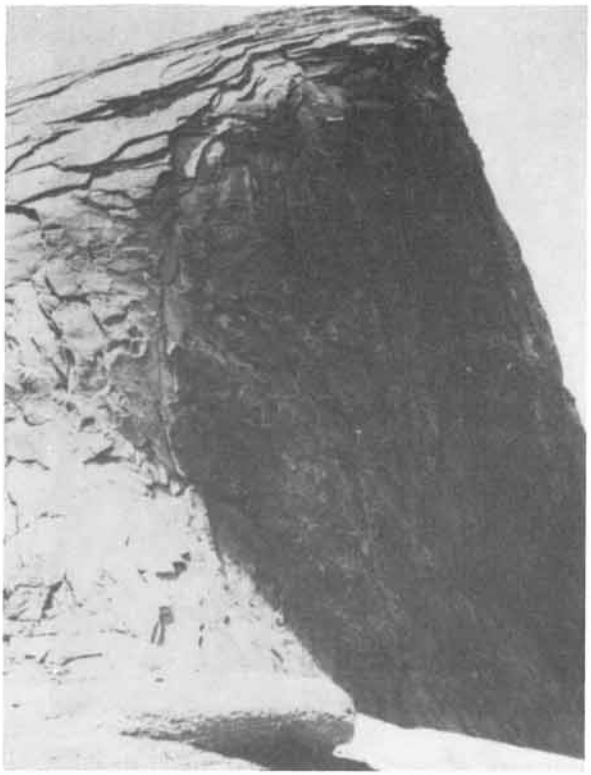

Figure 6-14a: *Sheeting of Half Dome, a granite pluton in Yosemite National Park, California.*

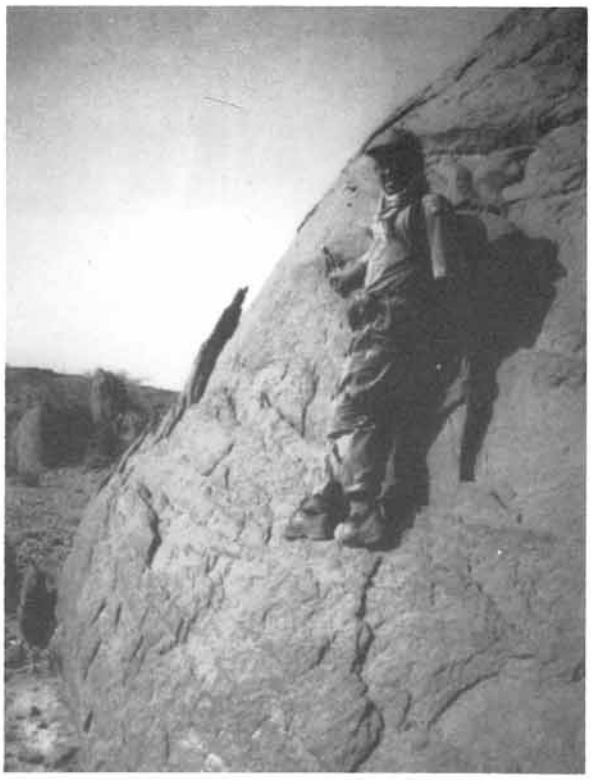

Figure 6-14b: *Exfoliation of granodiorite outcrop of the Mifsah pluton, Arabian Shield, Khamis Mushayt.*

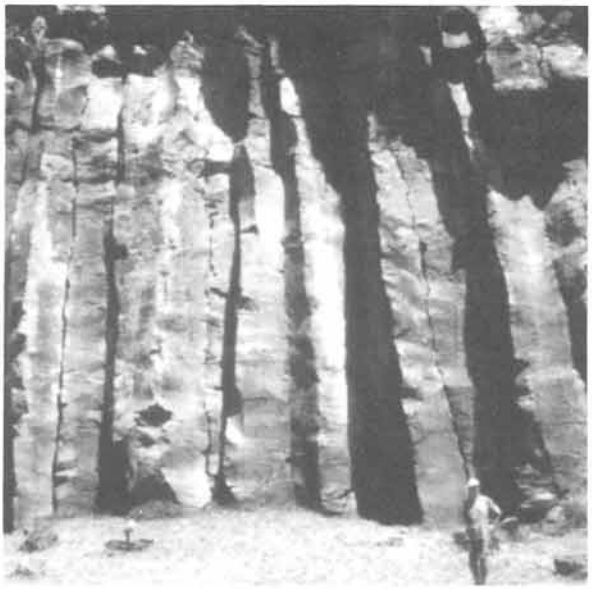

Figure 6-15a: *Massive columnar jointing in Tertiary basalt of Hells Gate National Park, African Rift Valley, Kenya.*

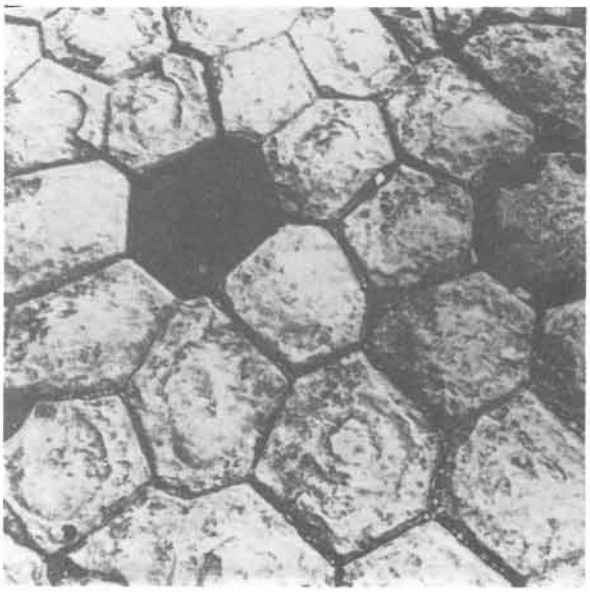

Figure 6-15b: *Top view of columnar joints in basalt sheet displays hexagonal pattern.*

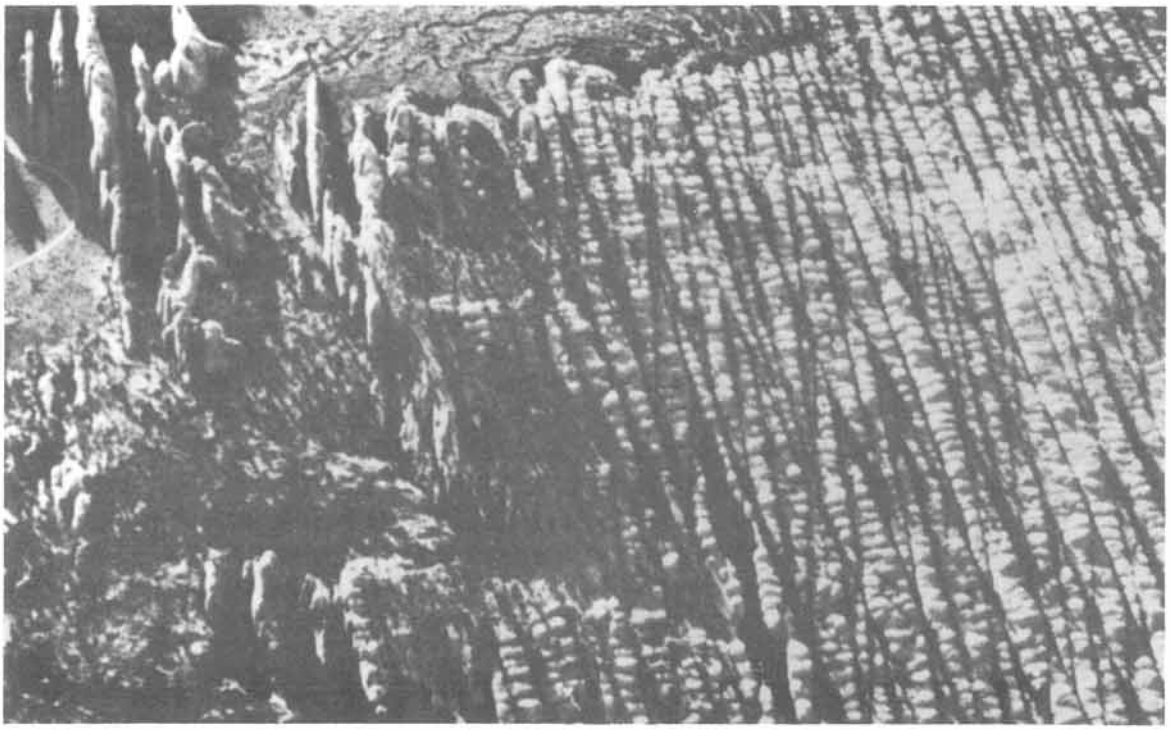

Figure 6-16a: *Oblique aerial view of two prominent sets of vertical joints in subhorizontal sandstones of the Entrada Formation, Moab, Utah.*

Figure 6-16b: *"Joint scape" of the Entrada sandstones have featured as a back drop in many movies.*

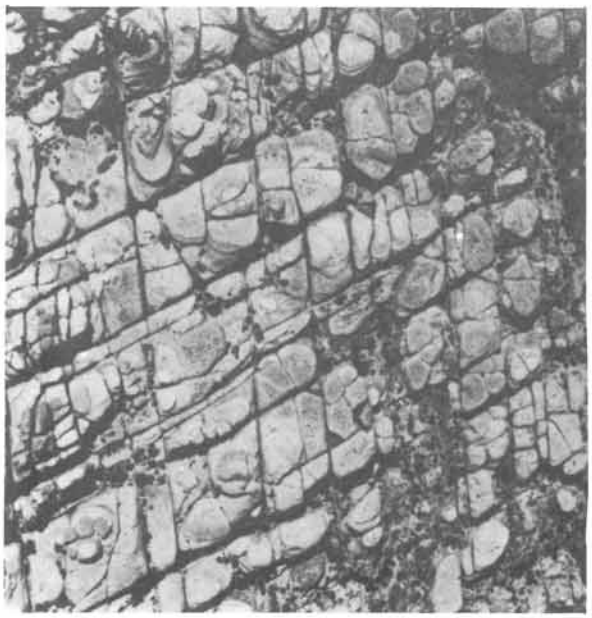

Figure 6-16c: *Orthogonal aerial view of vertical joint systems in horizontal sandstones of the Cedar Mesa Formation, Canyonlands National Park, Utah.*

□Exercise 6-7: Three joint systems, one following the tensile failure planes, complemented with the two conjugate shear joints, may form within buckle folds. The typical strain pattern in a buckle fold, deforming by layer-perpendicular pure shear strain, and the inferred stress trajectories are illustrated in Figures 6-17a & b. Indicate with a red pencil the orientation and likely location of tension and shear joints.

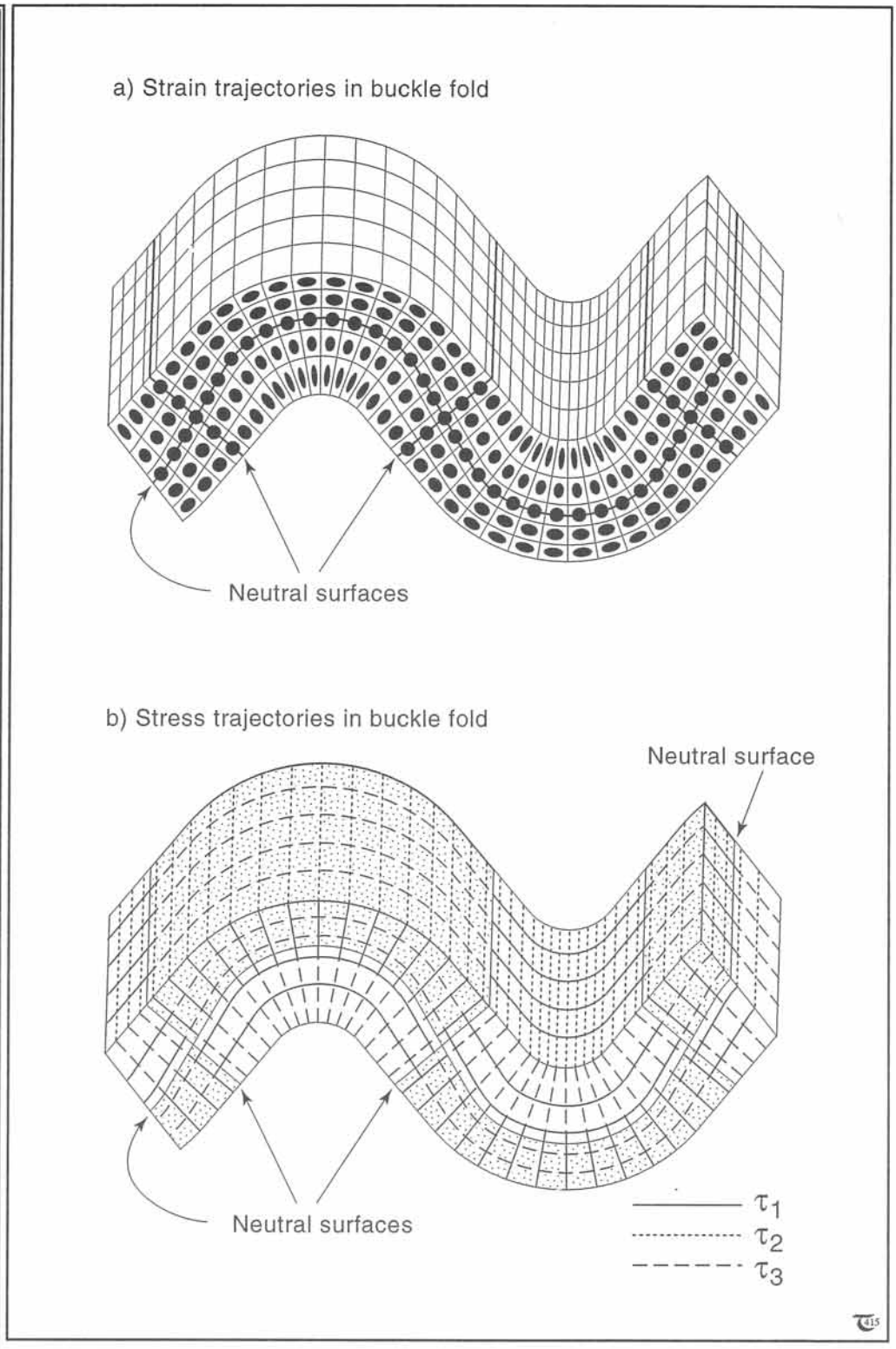

Figure 6-17: a) & b) Strain pattern and principal stress trajectories in buckle fold. See exercise 6-7.

6-6 Mohr-Coulomb yield criterion

Brittle failure and fault movement in rocks may occur in two possible fashions: either by the development of new fractures followed by slip or by immediate slip on pre-existing fractures. The formation of new fractures is associated with a drop in strength upon failure. The frictional strength on fault planes is normally constant. The creation of new fractures is governed by the Mohr-Coulomb yield criterion (termed, also, Navier-Coulomb criterion), whereas the shear stress required for frictional sliding on existing faults is described by Byerlee's law. This section concentrates on the Mohr-Coulomb criterion, and Byerlee's law is discussed in the next section.

A failure criterion is a specification of the state of stress at which failure occurs. An expression for the state of stress at failure was first introduced by Charles Coulomb in 1773:

$$\sigma_s = c_0 + \mu\sigma_N \qquad (6\text{-}1)$$

This equation takes into account an *inherent strength* or *cohesion*, c_0. The parameters c_0 and μ have to be determined in laboratory tests, using a range of confining pressures.

Equation (6-1) represents a family of lines, which are known as the *Mohr-Coulomb failure envelopes*. The slope of each failure envelope is given by the *coefficient of internal friction*, μ.

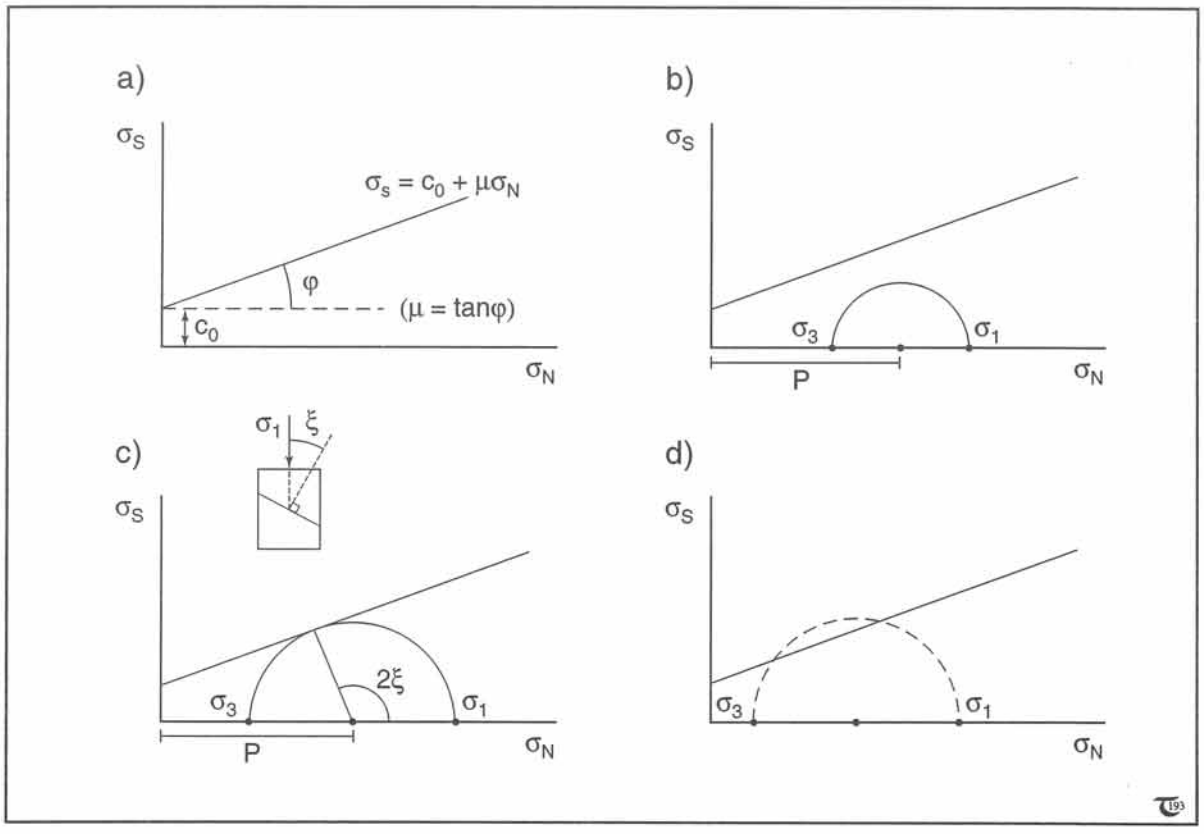

Figure 6-18: *a) to d) Mohr-Coulomb envelopes for brittle failure. (a) Definition sketch. (b) Possible state of stress, but too low for failure. (c) Critical stress state at failure; angle 2ξ fixes the orientation of the fault plane as shown. (d) Impossible state of stress, because the Mohr circle cannot cross the failure envelope.*

The actual orientation of the failure plane in the rock sample is, also, implied in μ. The angle ξ, indicated in Figure 6-18c, is measured between σ_1 and the normal to the failure plane. The critical angle of failure or angle of internal friction, ϕ, and the angle ξ, are related as follows:

$$\xi=(\pi/2)-(\phi/2) \qquad (6\text{-}2a)$$

$$\text{with: } \phi=\tan^{-1}\mu \qquad (6\text{-}2b)$$

Figure 6-18a graphs an example of a Mohr-Coulomb failure envelope, which uses the same axes as the Mohr diagram for total stress, outlined in section 4-4. The failure envelope separates two fields. The field inside the envelope represents stress states too small for brittle failure. The complementary field outside the envelope comprises theoretical pairs of shear stress and normal stress, which are never reached, be cause failure and the associated stress drop occur at the maximum strength, represented by the failure envelope. Figure 6-18b includes the Mohr circle for an arbitary uniform stress in a rock volume; this stress is too low to cause any brittle failure. Figure 6-18c illustrates a Mohr circle for a stress state, which is exactly that required for failure under confining pressure, implied by the offset of the Mohr circle from the axial origin. The state of stress portrayed in Figure 6-18d cannot be reached because failure and the associated drop in stress will occur long before this stress can be built up.

Figure 6-19 shows an example of the Mohr-Coulomb failure envelope, determined for Berea sandstone, deformed under isothermal conditions of 24° C, with a range of confining pressures as indicated by the Mohr circles for observed failure. The angle of fracture initiation is the same

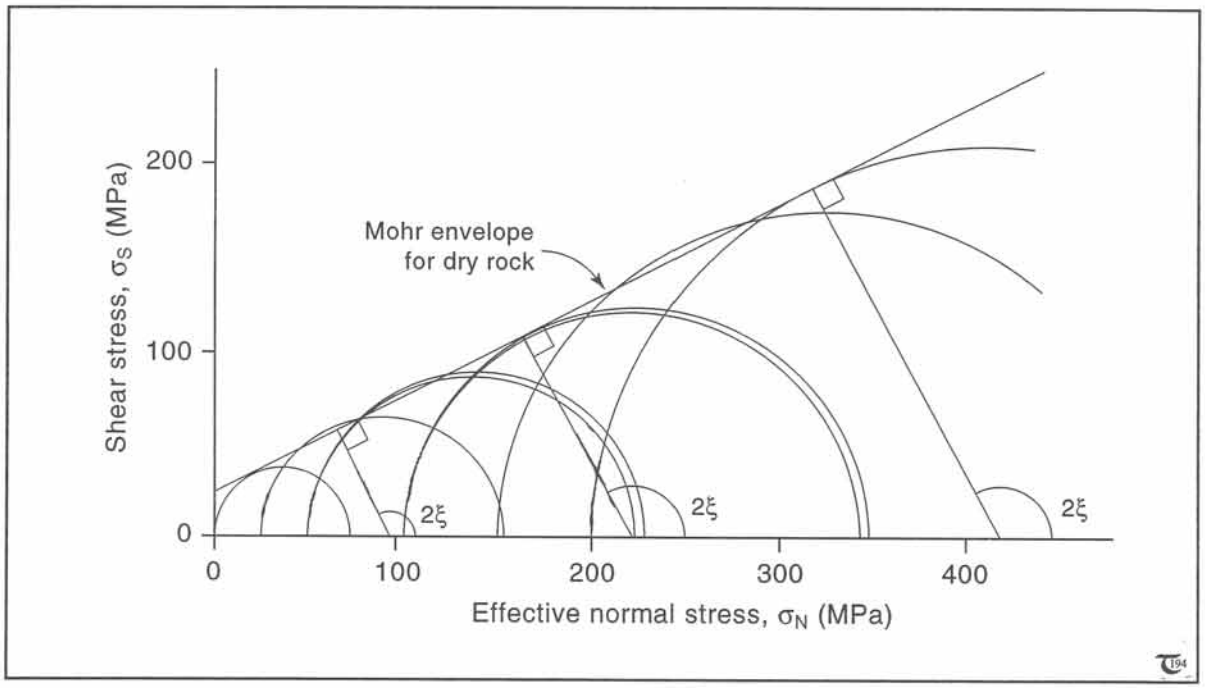

Figure 6-19: *Mohr envelope for Berea sandstone, established by drawing the best fit tangent to experimentally determined failure stresses at a range of confining pressures and isothermal conditions of 24° C.*

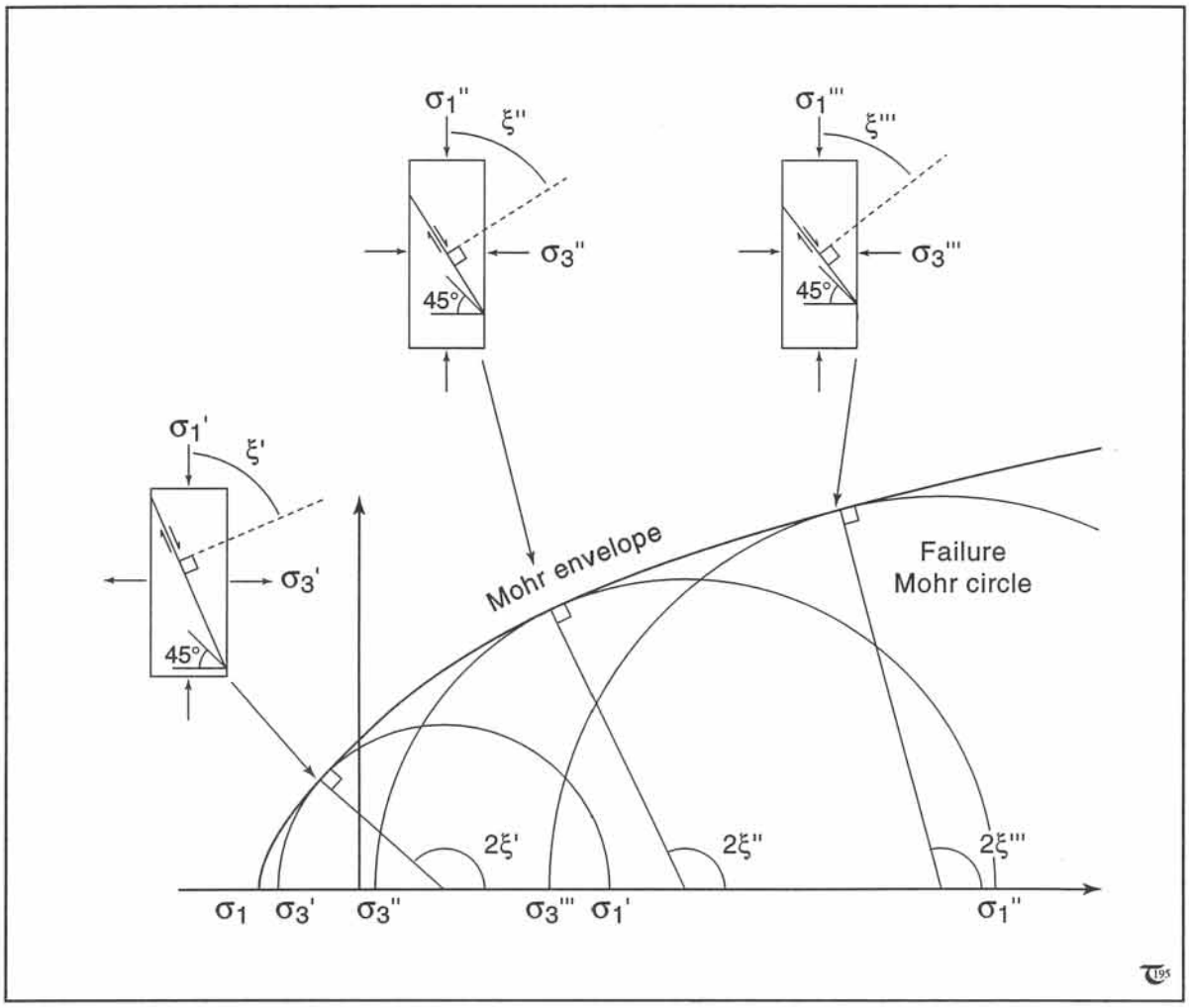

Figure 6-20: *Non-linear Mohr envelope for rock with pressure dependent failure angle, as indirectly given by 2ξ.*

for all pressures as the slope of the Mohr envelope is constant.

Although many rocks obey the linear failure criterion of Coulomb, similar to that portrayed for the Berea sandstone in Figure 6-19, some rocks deviate from the linear criterion. Figure 6-20 illustrates the empirical *Mohr envelope* for a rock, where the rate of strength increase decreases (that is, μ decreases), when the confining pressure increases. An immediate consequence of the departure from the Coulomb criterion is that the critical angle of failure changes gradually with the confining pressure. Tensile fractures are formed primarily at lower confining pressures, and the typical conjugate set of shear fractures preferentially form at higher confining pressures.

☐Exercise 6-8: Construct a Mohr-Coulomb envelope for pyroxenite, using the experimental data of Figure 6-9.

☐Exercise 6-9: a) Construct a Mohr-Coulomb diagram for Westerly granite: c_0=229 MPa and μ=1.4. b) Assume the granite occurs at 5 km depth and the pressure of the overburden is given by ρgz. Plot the state of effective pressure for three different fluid pressures: (1) hydrostatic fluid pressure, (2) fluid pressure of $0.8\rho gz$, and (3) fluid pressure equal to the lithostatic pressure. c) Consider that the region begins to undergo horizontal tectonic compression. Plot the successive states of stress as Mohr circles, finally plotting the Mohr circles for fault movement. What is the horizontal stress required to initiate fault movement for each of the fluid pressures considered? d) What are the dips and sense of displacement of the moving faults for each of the fluid pressures considered?

6-7 Amonton and Byerlee laws

The coefficient of internal friction, μ, on existing shear faults in *consolidated or "hard" rocks* determines which shear stress is required to cause further relative movement on the fault planes:

$$\sigma_S = \mu\sigma_N \qquad (6\text{-}3)$$

with normal and shear stresses, σ_S and σ_N, respectively. Equation (6-3), generally valid when two rough surfaces are in contact, is known as *Amonton's law*. The parameter μ, in this general sense, also, is referred to as the *coefficient of static friction*. The shear stress, required for activating frictional slip in hard rocks, is largely insensitive to the composition of the rock (Fig. 6-21a; compare to Fig. 3-4). The values determined for a variety of rocks fit a friction law with friction coefficient μ=0.85, using confining pressures corresponding to shallow crustal depths (up to 200 MPa or about 8 km depth):

$$\sigma_S = 0.85\sigma_N \qquad (6\text{-}4a)$$

Equation (6-4a) is valid for crustal depths from zero to eight kilometers. It appears that rocks deformed in the brittle regime, but at confining pressures in excess of 200 MPa, can better be described by including a parameter to express a non-linear reltionship between σ_S and σ_N (Fig. 6-21b):

$$\sigma_S = 60\ \text{MPa} + 0.6\sigma_N \qquad (6\text{-}4b)$$

Equation (6-4b) is valid for crustal depths beyond eight kilometers but above the brittle-ductile transition (see chapter eight, section 8-10). Equations (6-4a & b) for rock slip now are commonly referred to as *Byerlee's laws*.

The possible range of orientations for which slip on a pre-existing fracture is favored over development of new fractures through intact rock may be examined by comparing Byerlee's law with the Mohr-Coulomb envelope. Figure 6-22 illustrates the initial failure envelope and includes, also the frictional sliding envelope for Blair dolomite. The range of orientations suitable for frictional sliding over existing fractures is indicated in the dashed area. An existing fracture, inclined at 45° to σ_1, is not favored over the development of a new fracture at 22.5 to σ_1. However, a fracture inclined at 43° to σ_1 is equally likely to slip as a new fracture is to form. Frictional slip on pre-existing fractures in shallow rocks is, according to Byerlee's law, more important to brittle deformation than is the creation of new fractures. The effect of an increased pore pressure on the fault plane tends to reduce the normal stress and, consequently, reduces the shear stress required to cause fault slip.

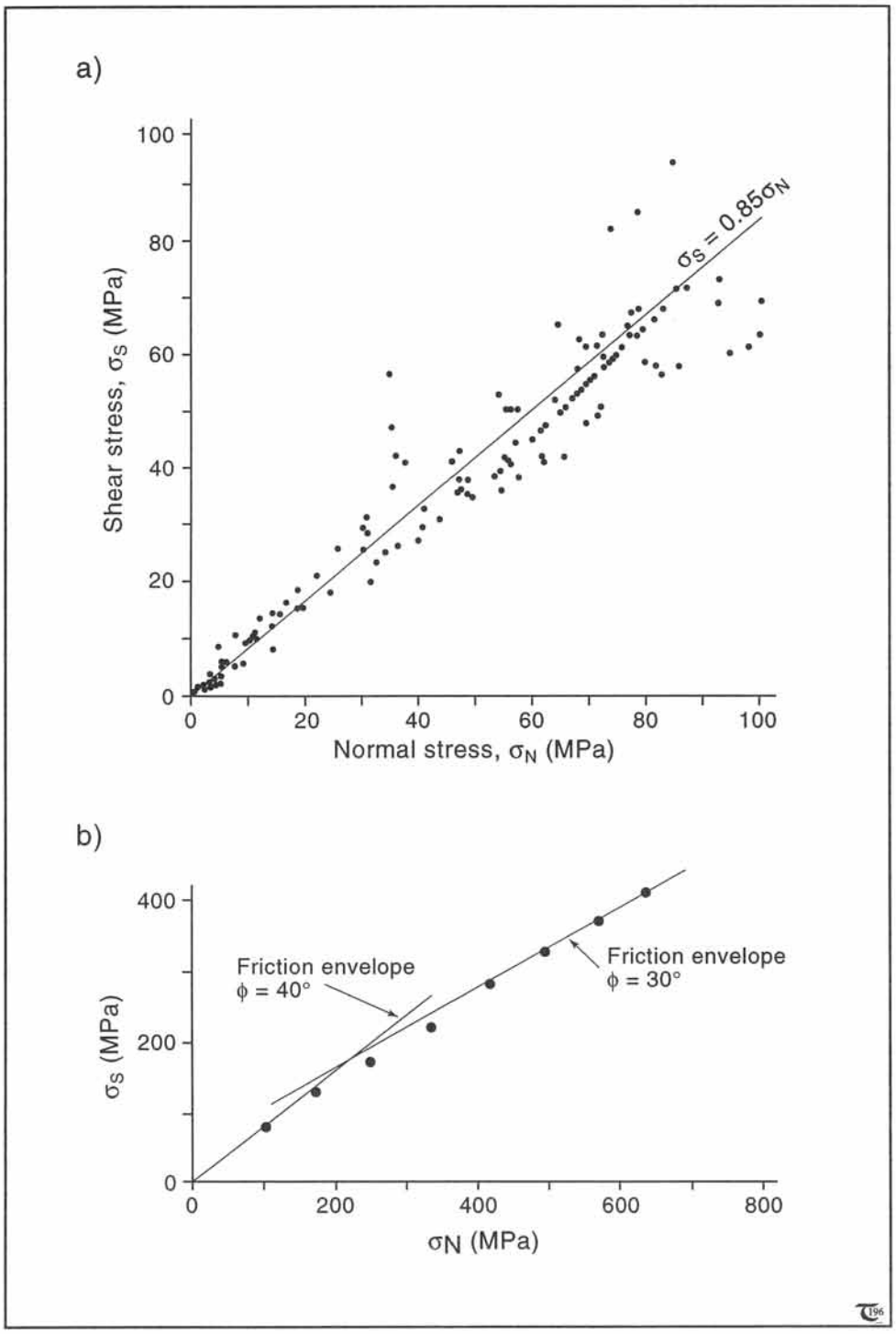

Figure 6-21: *a) & b) Byerlee graphs with stresses required to initiate slip in pre-fractured rocks, (a) up to 8 km deep, and (b) up to 30 km deep. See sections 8-9 and 8-10 for depths of brittle-ductile transition.*

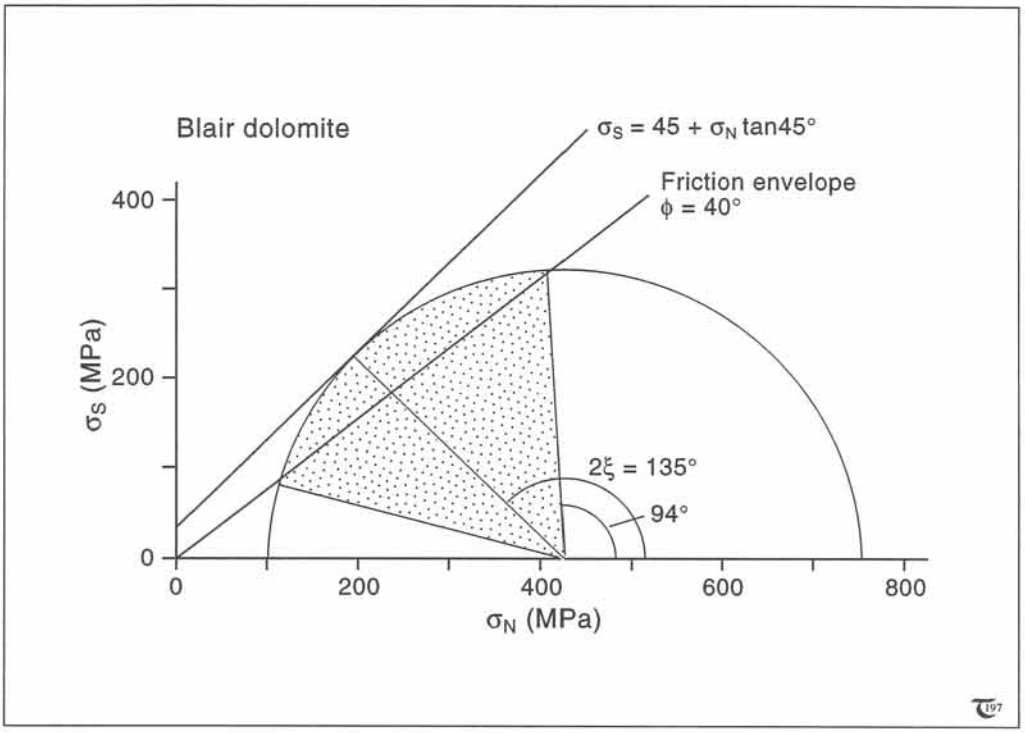

Figure 6-22: Comparison of initial failure envelope determined in Mohr-Coulomb tests and the Byerlee sliding envelope for Blair dolomite.

☐Exercise 6-10: Consider the stability of the rock slope, sketched in Figure 6-23, against sliding along the plane AB. Assume Amonton's law is applicable, and show that the condition for slope stability is tan $\alpha < \mu$.

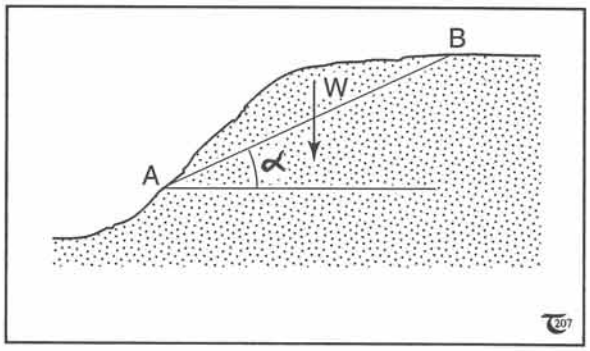

Figure 6-23: Principle sketch for exercise 6-10.

☐Exercise 6-11: The frictional strength envelope for most hard rocks obeys Byerlee's law. The state of total stress, confining pressure, and, thus, also, the deviatoric stress on the potential slide planes is completely determined for any critical Mohr circle. a) Draw the Byerlee failure envelope for shallow depths (<200 MPa). Scale both the horizontal and vertical axes in equal arbirary units of MPa. b) Draw various arbitrary Mohr circles, which are tangential to the failure envelope. c) Determine the angle between the failure planes and σ_1. d) Determine both the total normal stress and the deviatoric normal stress on the failure planes for, at least, six different confining pressures. Plot both stresses versus the pressure in a separate graph. Explain in physical terms how the graph should be interpreted.

6-8 Crustal strength in Andersonian faulting

Anderson linked, in 1942, the *orientation* of fault slip planes to the principal total stresses: one of the principal stresses is vertical, and the other two lie in the horizontal plane. Reverse and normal faulting have the intermediate principal stress axis parallel to the surface trace of the faults (Figs. 6-24a & b). Strike-slip faults have the intermediate stress axis normal to both the Earth's surface and the strike of the fault trace (Fig. 6-24c). For these principal cases of faulting, it is practical to reformulate the Mohr-Coulomb fracture criterion in terms of the total principal stress difference, instead of using the normal and

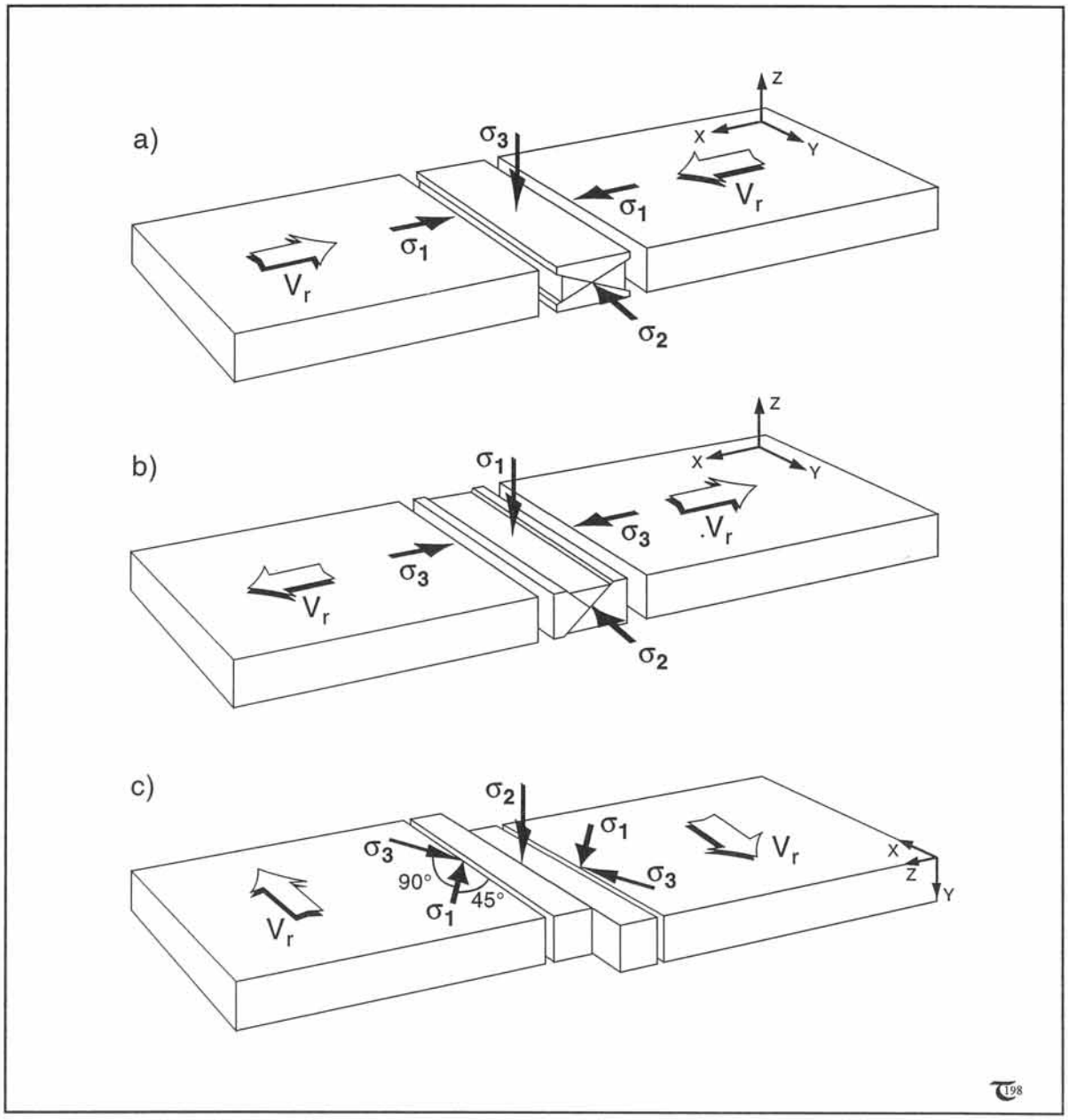

Figure 6-24: *a) to c) Three basic configurations of crustal faulting, according to Anderson: (a) reverse faulting, (b) normal faulting, (c) strike-slip faulting.*

shear stresses, as in equations (6-4a & b). The increase of the frictional strength with depth for normal, reverse, and strike-slip faults all will be different because of the difference in orientation with respect to the vertical stress. The governing equations for compressional (*shortening*), tensional (*extension*), and *strike-slip* faulting are, respectively:

$$(\sigma_1-\sigma_3)=\frac{2[c_0+\mu\rho gz(1-\lambda)]}{(\mu^2+1)^{1/2}-\mu} \qquad (6\text{-}5a)$$

$$(\sigma_1-\sigma_3)=\frac{-2[c_0-\mu\rho gz(1-\lambda)]}{(\mu^2+1)^{1/2}+\mu} \qquad (6\text{-}5b)$$

$$(\sigma_1-\sigma_3)=\frac{2[c_0+\mu\rho gz(1-\lambda)]}{(\mu^2+1)^{1/2}} \qquad (6\text{-}5c)$$

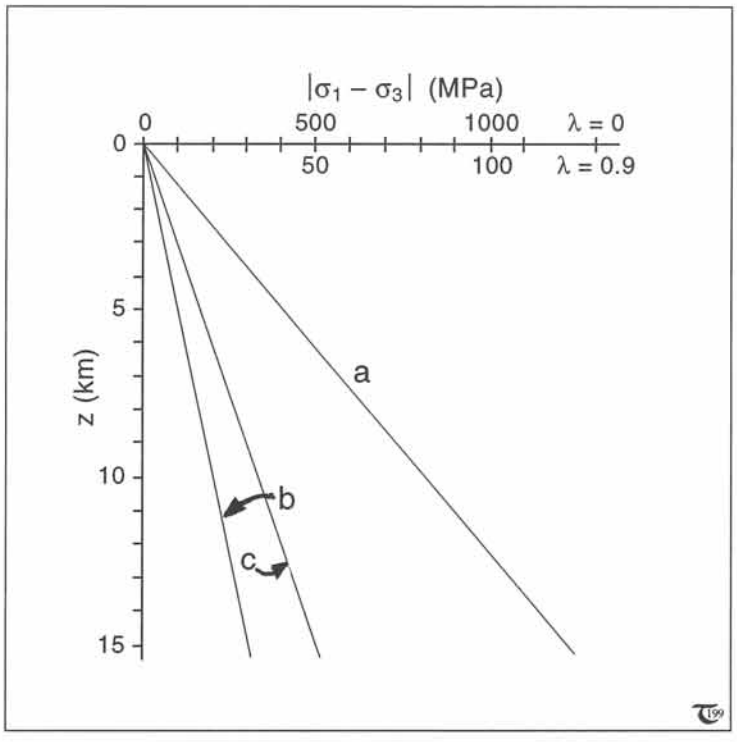

Figure 6-25: *Crustal strength in terms of differential stresses, required to initiate movement of (a) reverse faults, (b) normal faults, and (c) strike-slip faults. The differential stress axis is scaled for absence of pore water ($\lambda=0$) and super-hydrostatic pressures of $\lambda=0.9$.*

☐Exercise 6-12: Explain the meaning of the plot in Figure 6-25 in qualitative terms.

with principal total stresses, σ; cohesion, c_0; internal friction, μ; Hubbert-Rubey coefficient of fluid pressure, λ (see section 3-7); overburden density, ρ; gravitational acceleration, g; and depth, z, normal to the Earth's surface. Expressions (6-5a to c) specify which total differential stress is sufficiently large to activate fault-slip. These equations, also, show that the stress required for slip will be lower if the confining effect of lithostatic pressure is reduced by higher fluid pressure, which increases λ. *Minimum stress levels for movement on normal faults are only a quarter of those required for thrust faulting and about half that for strike-slip faulting (Fig. 6-25).*

6-9 Brittle strength envelopes for common rocks

Figure 6-26a shows strength profiles for dry rocks ($\lambda=0$) in tension and compression, using Byerlee's parameters in expressions (6-5a & b). Brittle yield envelopes are 87 MPa/km for dry compression and 19 MPa/km for dry (ex)tension. At deeper levels, these envelopes are cut off by the envelope 210 MPa+50 MPa/km for compression and 68 MPa+16 MPa/km for (ex)tension. Figure 6-26b shows the crustal strength profile for wet rocks in hydrostatic state ($\lambda=$ 0.42) in (ex)tension and compression. Brittle yield envelopes are 50 MPa/km for compression and 10 MPa/km for (ex)tension. At deeper levels, these envelopes change into the following envelopes: 210 MPa+29 MPa/ km for compression and 68 MPa+ 9 MPa/km for (ex)tension, assuming hydrostatic pore pressure ($\lambda=$ 0.42).

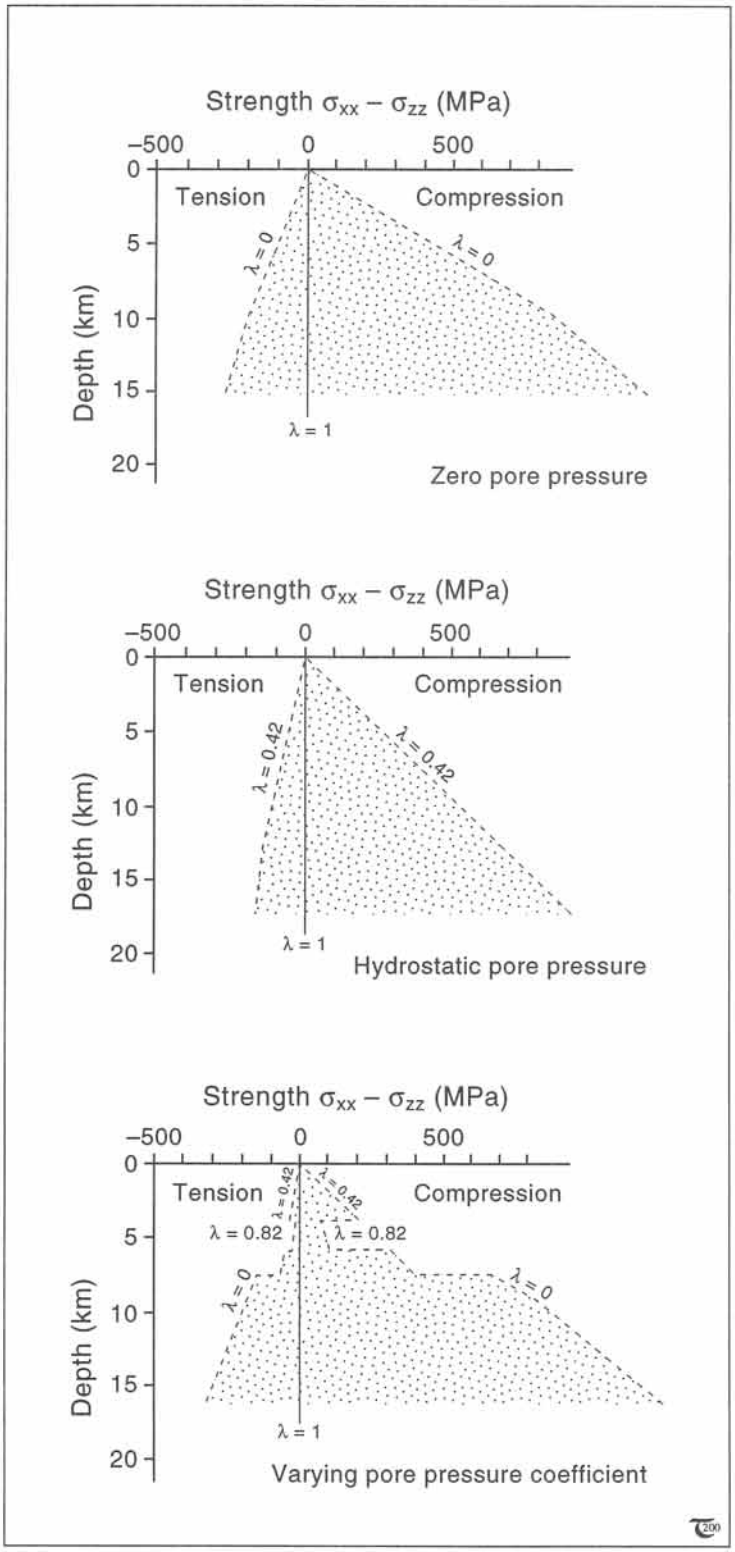

Figure 6-26: a) to c) Crustal strength profiles for brittle rocks at: (a) zero pore pressure, (b) hydrostatic pore pressure, and (c) pore pressure varying with depth as shown.

Figure 6-26c illustrates that abrupt changes in pore pressure may cause large jumps in the strength profile for shallow crustal rocks. Abrupt vertical changes in pore pressure are as follows: hydrostatic above 4 km ($\lambda=0.42$), overpressured between 4 and 6 km ($\lambda=0.82$), hydrostatic between 6 and 8 km ($\lambda=0.42$), and zero in the absence of significant water below 8 km ($\lambda=0$). Brittle yield envelopes are $87(1-\lambda)$ MPa/km for compression and $19(1-\lambda)$ MPa for (ex)tension. At deeper levels, these envelopes are cut off by the envelope 210 MPa$+50(1-\lambda)$ MPa/km for compression and 68 MPa$+16(1-\lambda)$ MPa/km for (ex)tension.

☐Exercise 6-13: Figure 6-27a graphs the general frictional strength envelope of crustal hard rocks, both for compression and tension and a variety of fluid pressures. In a particular ultra-deep well, the variation of the fluid pressure inside the penetrated rock formations has been carefully logged, as in Figure 6-27b. Use the nomogram of Figure 6-27a to construct the crustal failure envelope, that shows the resistance to frictional sliding at various depths in the logged hole, both for times of regional compression and for times of regional extension.

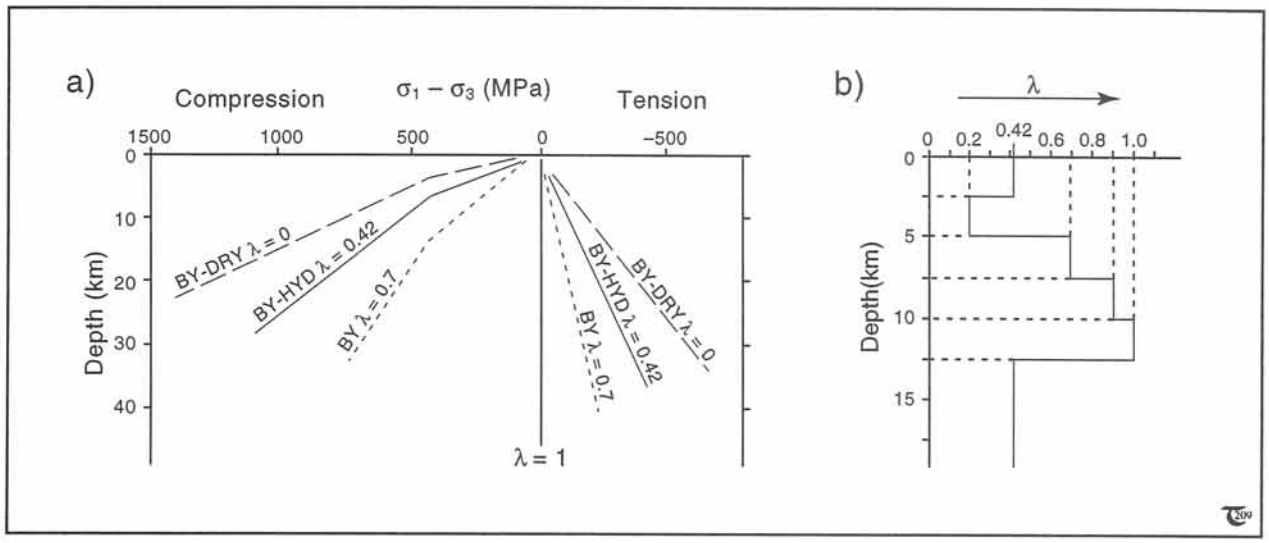

Figure 6-27: *a) Frictional strength envelope for crustal rocks. b) Example of pore water pressure changes recorded in a bore hole. See exercise 6-13.*

References

Advanced texts on the faulting and fracture mechanics of rocks include the following:

A. Books

The Dynamics of Faulting and Dyke Formation with Applications to Britain (1951, Oliver and Boyd, 206 p.), by E.M. Anderson. A classical treatise on the orientation of the principal stresses during faulting.

Engineering Behaviour of Rocks (1968, Chapman and Hall, 208 pages), by Ian Farmer. An easy text for undergraduate students.

Experimental Rock Deformation - The Brittle Field (1978, Springer-Verlag), by M.S. Paterson. A classical text on brittle failure by a distinguished experimentalist.

Fracture Mechanics of Rock (1987, Academic Press), edited by B.K. Atkinson. This work contains some very specialized papers of high quality research in the field of brittle rock mechanics.

Mechanics of Tectonic Faulting (1988, Elsevier, 351 pages), by G. Mandl. This book contains a lot of theoretical concepts, related to the faulting of rock.

The Fracture of Rocks (1988, North Oxford Academic Press), by J.-L. Blès and B. Feuga. Translated from French by J. Wanklyn.

Introduction to Rock Mechanics (1988, Wiley), by R. Goodman. An established textbook, well-written, and detailed account on brittle rock mechanics.

The Mechanics of Earthquakes and Faulting (1990, Cambridge University Press), by C.H. Scholz.

Fault Mechanics and Transport Properties in Rocks (1992, Academic Press, 536 pages), edited by B. Evans and T.-F. Wong. This is a collection of papers by a variety of individual authors. They cover topics, such as the brittle strength of rocks, stress-induced damage in rocks, permeability and pore flow, and the role of stress in tectonic processes.

Rock Mechanics on a Geological Base (1995, Elseviers, 518 pages) by R. Pusch. This book is intended for geologists involved with engineering and waste disposal programs.

B. Articles

The following articles provide useful complementary reading to the topics discussed in this chapter:

Byerlee, J.D. (1968, *Journal of Geophysical Research*, volume 73, pages 4,741 to 4,750). Brittle-ductile transition in rocks.

Byerlee, J.D. (1975, *International Journal of Rock Mechanics and Mining Science*, volume 12, pages 1 to 4). The fracture strength and frictional strength of Weber sandstone.

Byerlee, J.D. (1978, *Pure and Applied Geophysics*, volume 116, pages 615 to 626). Friction of rocks.

Engelder, T. and Marshak, S. (1988, chapter 10 in Marshak, S. and Mitra, G., *Basic Methods of Structural Geology*, 450 pages). Analysis of data from rock-deformation experiments.

Fatt, I. (1958, *American Association of Petroleum Geologists Bulletin*, volume 42, pages 1924 to 1957). Compressibility of sandstones at low to moderate pressures.

Handin, J., Hager, R.V., Friedman, M., and Feather, J.N. (1963, *American Association of Petroleum Geologists Bulletin*, volume 47, pages 717 to 755). Experimental deformation of sedimentary rocks under confining pressure: pore pressure tests.

Lockner, D.A. (1995, In: *Rock Physics and Phase Relations*. Ed. T.J. Ahrens. AGU, Washington, pages 127 to 147). Rock Failure.

Paterson, M.S. (1987, *Tectonophysics*, volume 133, pages 33 to 43). Problems in the extrapolation of laboratory rheological data.

Paterson, M.S. and Weiss, L.E. (1966, *Geological Society of America Bulletin*, volume 77, pages 343 to 374). Experimental deformation and folding in phyllite.

Sibson, R.H. (1974, *Nature*, volume 249, pages 542 to 544). Frictional constraints on thrust, wrench, and normal faults.